Applied Catalysis B: Environmental 343 (2024) 123503

Contents lists available at ScienceDirect

Applied Catalysis B: Environmental

journal homepage: www.elsevier.com/locate/apcatb

# Operando induced strong metal-support interaction of $Rh/CeO_2$ catalyst in dry reforming of methane

Yuvaraj Gangarajula [a,1], Feng Hong [a,1], Qinghe Li [a], Xunzhu Jiang [a,b], Wei Liu [c], Mohcin Akri [a], Yang Su [a], Yanjie Zhang [d,*], Lin Li [a,*], Botao Qiao [a,*]

[a] CAS Key Laboratory of Science and Technology on Applied Catalysis, Dalian Institute of Chemical Physics, Chinese Academy of Sciences, Dalian 116023, China
[b] University of Chinese Academy of Sciences, Beijing 100049, China
[c] Division of Energy Research Resources, Dalian National Laboratory for Clean Energy, Dalian Institute of Chemical Physics, Chinese Academy of Sciences, Dalian 116023, China
[d] Research Institute of Photonics, Dalian Polytechnic University, Dalian 116034, China

ARTICLE INFO

*Keywords:*
$CO_2$-treatmennt
Dry reforming of methane
Methane activation
Strong metal-support interaction
Operando structure evolution

ABSTRACT

Strong metal-support interaction (SMSI) is an important concept in heterogeneous catalysis that has a profound effect on the structure and activity of the supported metal catalyst. However, the catalyst with an uncontrolled SMSI state significantly prevents the accessibility of metal surface to reactants by encapsulation process which inevitably limits their practical application. Herein, we demonstrate that under the reaction condition of dry reforming of methane (DRM), the occurrence of SMSI ($CO_2$-SMSI) can be operando induced between Rh and $CeO_2$ which significantly improves the catalytic activity in DRM reaction. Detailed study has revealed that the formation of suitable $Rh^{\delta+}/Rh^0$ species in $CO_2$-SMSI is critical in improving $CH_4$ activation, while the presence of permeable encapsulation layer is helpful to provide more active sites. This discovery provides a new approach to overcome the limitation of classical SMSI catalyst in DRM reaction.

## 1. Introduction

Dry reforming of methane (DRM) is an effective approach to convert two most important greenhouse gases, i.e., $CO_2$ and $CH_4$, into industrial syngas with desired ratio ($H_2$/CO ratio = ~1) required for the synthesis of liquid hydrocarbons, oxygenates and fuel through Fischer-Tropsch synthesis [1–8]. However, the highly endothermic nature of DRM reaction demands elevated operating temperature to attain better conversion where the catalyst tends to deactivate by metal sintering and uncontrolled coke deposition [9–16]. Therefore, the lack of reliable catalyst limits the industrialization of the DRM process [17,18]. Among the catalysts reported for DRM reaction [19], supported Rh seems to be the best which exhibits high activity with strong resistance for coke deposition [20,21]. However, variety of studies have revealed that the catalytic performance of supported Rh catalysts is significantly influenced by support characteristics [22,23]. For example, inert support (often irreducible metal oxides) supported Rh catalysts exhibit lower stability than reducible oxide supported ones due to the relatively weak metal-support interaction [24]. On the other hand, compared with irreducible oxides, the initial activity of reducible metal oxides (such as $TiO_2$, $CeO_2$, $ZrO_2$, $Ta_2O_5$ and $Nb_2O_5$) supported Rh catalysts is low, most probably due to the Rh surface was covered by partially reduced support species through strong metal-support interaction (SMSI) effect [23,25].

Tauster et al. first discovered the SMSI phenomenon in the late 1970s on $TiO_2$ supported platinum group metals (PGMs) upon high-temperature reduction (HTR) treatment, where PGMs lost their ability to adsorb small molecules such as CO and $H_2$ and such an unusual change in chemisorption property is ascribed to electronic effect and formation of encapsulation layer on PGMs [26–32]. The SMSI effect is useful in stabilizing active metals, tuning catalytic performance and exploring reaction mechanism [33]. Therefore, in recent years it gains renewed attention, and various new types of SMSI have been successively discovered [27,34–40]. It was found that the nature of the support determines, at least to a large extent, the atmosphere under which the SMSI state manifests [34,36,37,41–43]. However, the general opinion on the classical SMSI phenomenon is that an uncontrolled SMSI state decreases the exposed active metal surface by the formation of complete encapsulation layer on metal NPs and prevents the metal surface access

* Corresponding authors.
*E-mail addresses:* zhang_yj@dlpu.edu.cn (Y. Zhang), llin@dicp.ac.cn (L. Li), bqiao@dicp.ac.cn (B. Qiao).
[1] These authors contributed equally to this work.

https://doi.org/10.1016/j.apcatb.2023.123503
Received 9 July 2023; Received in revised form 8 November 2023; Accepted 9 November 2023
Available online 11 November 2023

to the reactants [37,44,45]. To design catalyst with higher activity and stability, the degree of encapsulation layer has been successfully optimized by a few approaches, such as nanoscale architectural design (Au/HAP-$TiO_2$), permeable/porous encapsulation layer (SMSI on Au/$TiO_2$ with melamine), Au/$TiO_2$ with wet chemistry SMSI and adsorbate mediated SMSI on Rh/$TiO_2$, Rh/$Nb_2O_5$ and Ni/h-BN [27,36, 45,46]. However, the formation of permeable encapsulation layer on metal surface with SMSI state is limited to few supported metal catalysts and it remains a major challenge in the field of heterogeneous catalysis.

Here we demonstrate the manifestation of SMSI between Rh and $CeO_2$ upon $CO_2$ treatment at high temperature which exhibits significantly enhanced catalytic activity. Detailed characterization combined with control experiments reveal that $CO_2$-SMSI catalyst consists of subtle $Rh^{\delta+}/Rh^0$ mixture along with permeable encapsulation layer on Rh NPs which are responsible for the exceptional activity in DRM reaction. Therefore, $CO_2$-SMSI state helps to overcome the limitation of both electronic and encapsulation layer associated with classical SMSI catalyst.

## 2. Experimental details

Rhodium nitrate (Aldrich, ~36 % Rh), Ruthenium chloride (Tianjin Fengchuan Chemical Reagent Co., Ltd), $CeO_2$ (Sinopharm Chemical Reagents, 3.5 N) were used without further purification.

### 2.1. Catalysts preparation

Synthesis of 0.1 wt% Rh/$CeO_2$ catalyst by wet impregnation method.

$CeO_2$-supported Rh catalyst with 0.1 wt% of Rh was prepared by a wet impregnation method. 1 mL rhodium nitrate solution (containing 1 mg of Rh) was added into 100 mL of distilled water and stirred for 20 min. 1 g of $CeO_2$ support was added and stirred for 4 h at room temperature and then filtered, washed with distilled water and dried at 80 °C for 12 h. The obtained dried mass was calcined at 500 °C for 4 h. The sample of 0.1 wt% Ru/$CeO_2$ catalyst was prepared by the same method.

Synthesis of cerium dioxide by thermal decomposition method (homemade $CeO_2$).

Cerium dioxide was synthesized by decomposition of cerium nitrate hexahydrate (Aladdin, 99 %) in muffle furnace at 700 °C for 4 h and wet impregnation method was used to deposit 0.1 wt% of Rh on $CeO_2$ using appropriate quantity of rhodium nitrate.

### 2.2. Characterization

In order to identify the amount of metal present in the catalyst, inductively coupled plasma -atomic emission spectroscopy (ICP-AES, IRIS Intrepid II XSP instrument (Thermo Electron Corporation)) analysis has been carried out.

The in-situ diffuse reflectance infrared Fourier transform spectra (DRIFTS) analysis of the samples were performed on a Bruker Vertex 70 V FTIR spectrometer equipped with a MCT detector and operated at a resolution of 4 $cm^{-1}$ using 32 scans. Before CO adsorption studies, the in-situ pretreatment was carried out with 5 vol% $H_2$/He (at 200 °C and 850 °C for 1 h) and pure $CO_2$ gas (at 850 °C for 1 h) with flow rate of 30 mL/min separately and then cooled to room temperature. Later, the samples were purged with He for 10 min and then background spectra was recorded. Then CO adsorption study was carried out with 1 vol% CO balanced with He gas (30 mL/min) at room temperature. Subsequently, the spectra were collected until there was no change in the absorbance.

To confirm the oxidation sate of Rh in Rh/$CeO_2$-850-$CO_2$ catalyst during DRM reaction, the Rh/$CeO_2$ catalyst was subjected to in-situ $CO_2$-pretreatment at 850 °C for 1 h (pure $CO_2$, 30 mL/min) in DRIFTS cell, then the temperature decreased to 700 °C, subsequently the sample was purged with He gas for 10 min. Later, DRM reaction was carried out at 700 °C (700 °C was used on account of the limit of the equipment) for 3 h by sending feed gas ($CH_4$: $CO_2$ = 1, 30 mL/min). After 3 h of DRM reaction, sample was cooled to room temperature with He gas purging and background spectra was recorded. Then CO adsorption study was carried out using 1 vol% CO/He gas (30 mL/min) and spectra was recorded until no changes in the CO adsorption and then desorption with He gas was carried out.

DRIFT experiments for in-situ $CO_2$ or CO adsorption over Rh/$CeO_2$ was conducted in the same instrument mentioned above. The sample was subjected to the purge with He gas (30 mL/min) at room temperature for 0.5 h, and then a background spectrum was collected from the fresh Rh/$CeO_2$ using 64 scans and 4 $cm^{-1}$ resolution. After that, the adsorption gas was changed to pure $CO_2$ or CO, and the DRIFT spectra were obtained by subtracting the background spectrum from subsequent spectra and are reported herein. The measurements were performed at room temperature, 100°C, 200°C, 300 °C, 400 °C, and 500 °C, respectively. In the experiment of CO adsorption, the spectra were recorded after the gaseous CO was removed by He purge to avoid the interference of signal of CO adsorption on Rh/$CeO_2$.

To confirm the size and dispersion of metal particles of the catalysts, high resolution transmission electron microscopy (HRTEM) analysis of all the samples were carried out using JEOL JEM-2100 F microscope. To determine the composition of the encapsulation layer on Rh NPs on $H_2$- and $CO_2$-pretreated catalysts, in-situ EELS analysis has been carried out on Titan Themis G3 (Titan-ETEM, Thermo Fischere Scientific Company). The Titan-ETEM works at 300 kV with a spherical-aberration (Cs) corrector for parallel imaging (CEOS GmbH) and measured resolution of better than 0.1 nm. Before analysis, the samples were pretreated with $CO_2$ atmosphere (2.7 mbar, 30 mL/min) at 850 °C (heating rate 10 °C/s by DENS heating holder) in ETEM chamber with a self-developed gas system. The sample was pretreated for 90 min at 850 °C and then, the image acquired in $CO_2$ atmosphere (0.1 mbar) at 300 °C. Similar procedure were followed for $H_2$-pretreated sample to acquire images. STEM imaging was adopted to get high-quality EELS data. The convergence and EELS collection signals were 13.7 mrad and 24.2 mrad respectively at 300 kV. We set the camera at the length of 60 mm and a condenser aperture of 70 μm. EELS spectra were acquired in Dual EELS mode allowing for the precise calibration of the peak. EELS data was acquired with an energy dispersion of 0.5 eV/pixel and acquisition time of 0.1 s/pixel. EELS datasets were processed by using Digital Micrograph.

The in-situ X-ray photoelectron spectroscopy (XPS) analysis of all Rh/$CeO_2$ catalysts were performed on a Thermo Fisher Scientific Brno XPS machine equipped with an atmospheric reaction chamber. The energy source used in this study is Al Kα characteristic X-ray line, 30 eV pass energy (energy steps 0.050 eV) and standard mode were applied for recording the XPS lines of Rh species. Samples were heated in the atmospheric reaction chamber attached to the high vacuum space of the instrument. Pretreatment was performed separately in $H_2$ atmospheres at 200 °C, 850 °C and $CO_2$ pretreatment at 850 °C for 1 h with ramp rate of 10 °C/min. And then the samples were cooled to room temperature, transferred into the analysis chamber that was evacuated to $4 \times 10^{-10}$ torr before spectral acquisition. Spectral processing was performed using Thermo Adantage software. The binding energy of all the samples were calibrated with C 1 s binding energy 284.8 eV.

### 2.3. Catalytic test

Catalytic performance of the synthesized catalysts was investigated in the dry reforming of methane reaction. Before the catalytic test, the catalyst (50 mg) was pretreated with pure $H_2$, CO, $CH_4$ and $CO_2$ at different temperatures (200 °C, 700 °C and 850 °C as per requirement) for 1 h followed by He gas purging for 15 min. The catalytic test was conducted in the temperature range of 600–850 °C under atmospheric pressure using the feed gas composition of $CH_4$: $CO_2$ = 1:1 with gas hourly space velocity (GHSV) of 36000 mL $g_{cat}^{-1}$ $h^{-1}$. The effluent gas concentrations were analyzed by an Agilent 6890 GC analyzer equipped with a TDX-01 column and a thermal conductivity detector. The

conversion of $CH_4$ and $CO_2$ were calculated according to the following formula:

$X_{CH4} = ([CH_4]_{in}-[CH_4]_{out})/[CH_4]_{in} \times 100\ \%$

$X_{CO2} = ([CO_2]_{in}-[CO_2]_{out})/[CO_2]_{in} \times 100\%$

$H_2/CO = [H_2]_{out}/[CO]_{out}$

Where $[CH_4]$ and $[CO_2]$ are in molar concentration. Specific activity for $CH_4$ and $CO_2$ on Rh/$CeO_2$-850-$H_2$ and Rh/$CeO_2$-850-$CO_2$ catalysts (mol. $g_{Rh}^{-1}h^{-1}$) was calculated using the following formula [2].

$R(CH_4) = (\text{Moles of } CH_4 \text{ converted})/(\text{Catalyst weight} \times W_{Rh}) \times 60$

$R(CO_2) = (\text{Moles of } CO_2 \text{ converted})/(\text{Catalyst weight} \times W_{Rh}) \times 60$

where, moles of $CH_4$ converted $= ([\text{Total flow of } (CH_{4,\ in}) \times X_{CH4}])/22400$

moles of $CO_2$ converted $= ([\text{Total flow of } (CO_{2,\ in}) \times X_{CO2}])/22400$

Where, $(CH_4)$ and $(CO_2)$ - the concentration of $CH_4$ and $CO_2$ respectively (in moles); $X(CH_4)$ and $X(CO_2)$ - conversion of $CH_4$ and $CO_2$ respectively; and $w_{Rh}$ – Rh loading (wt%).

Turnover frequency (TOF) = specific rate x $M_{Rh}$ /Dispersion /3600. Rh dispersion was calculated using the following formula.

$D(\%) = 1{\cdot}0092/d_{VA}$

where $d_{VA}$ indicates average size of Rh nanoparticles.

## 3. Results and disscusion

### 3.1. Activity evaluation of different catalysts

Commercial $CeO_2$ was used as support without further modification and we will show later that homemade $CeO_2$ also works. $CeO_2$ supported Rh catalysts were prepared by an impregnation method with a nominal Rh weight loading of 0.1 wt%, followed by calcination at 500 °C for 4 h. The detailed catalyst preparation procedure is given in the support information (SI). The ICP-AES result (Table S1 in SI) shows that actual loading of Rh in Rh/$CeO_2$ catalyst is 0.07 wt%, slightly lower than the nominal one.

Prior to catalytic performance test for DRM reaction, Rh/$CeO_2$ catalyst was subjected to in situ $H_2$ pretreatment at 200 °C for 1 h, denoted as Rh/$CeO_2$-200-$H_2$. As shown in Fig. 1a and b, the catalyst shows a very low initial activity (~17% $CH_4$ conversion and ~37 % $CO_2$ conversion). However, the conversion increases gradually to higher than 80 % with reaction time evaluation, accompanied by a significant increase of $H_2$/CO ratio (from ~0.09 to ~0.65, Fig. 2a). A similar trend was observed on the calcined Rh/$CeO_2$ catalyst without reduction (denoted as Rh/$CeO_2$-fresh). Such a significant catalytic performance change must have originated from the catalyst structure or property evolution under reaction condition, most probably due to the effect of reaction and/or product gas. We therefore screened the plausible effect of single reaction and product gases first: We treated the sample by pure $CH_4$, $CO_2$, CO and $H_2$ at 850 °C for 1 h (denoted as Rh/$CeO_2$-850-$CH_4$, Rh/$CeO_2$-850-$CO_2$, Rh/$CeO_2$-850-CO and Rh/$CeO_2$-850-$H_2$, respectively), and then conducted the catalytic test. As shown in Fig. 1c and d,

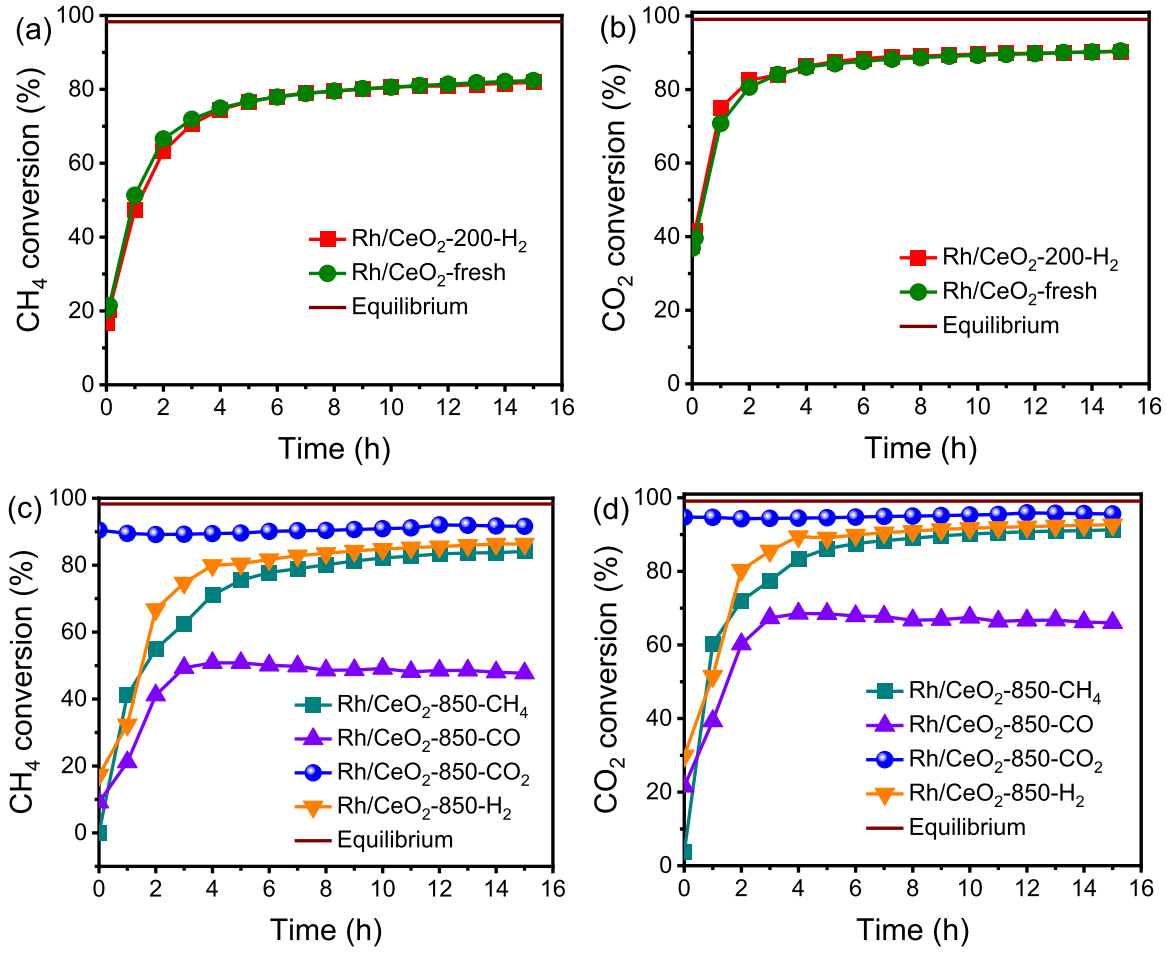


**Fig. 1.** (a, b) $CH_4$ and $CO_2$ conversion on Rh/$CeO_2$-fresh and Rh/$CeO_2$-200-$H_2$ catalysts in DRM reaction at 850 °C; (c, d) $CH_4$ and $CO_2$ conversion on $CH_4$-, $CO_2$-, CO- and $H_2$-pretreated-Rh/$CeO_2$ catalysts in DRM reaction at 850 °C.

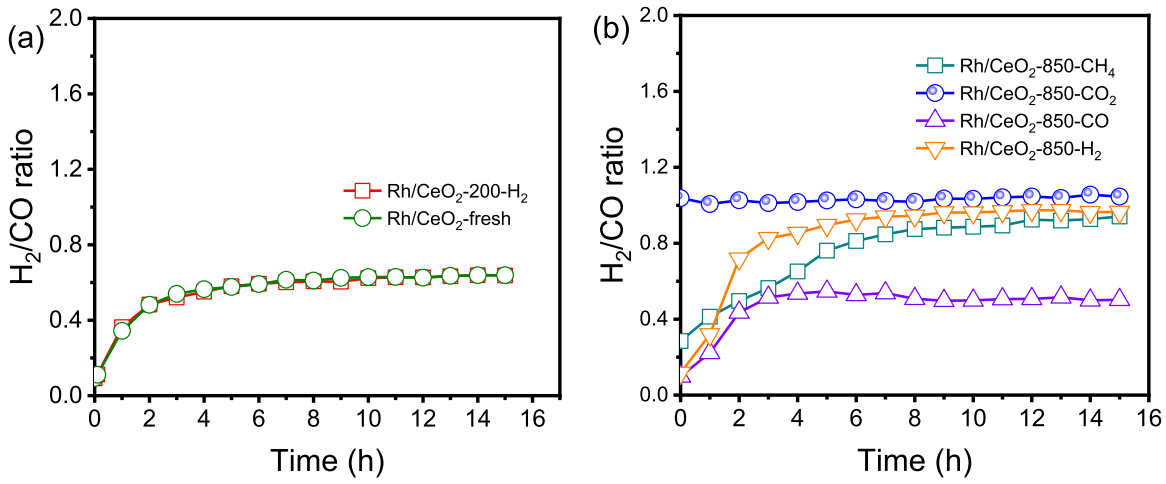


**Fig. 2.** (a) $H_2$/CO ratio on Rh/$CeO_2$-fresh and Rh/$CeO_2$-200-$H_2$ catalysts in DRM reaction at 850 °C; (b) $H_2$/CO ration on Rh/$CeO_2$-850-$CH_4$, Rh/$CeO_2$-850-CO, Rh/$CeO_2$-850-$CO_2$ and Rh/$CeO_2$-850-$H_2$ catalysts in DRM reaction at 850 °C.

Rh/$CeO_2$-850-$CH_4$, Rh/$CeO_2$-850-CO and Rh/$CeO_2$-850-$H_2$ catalysts display similar scenario of the low initial activity increasing gradually with reaction time. On the contrary, Rh/$CeO_2$-850-$CO_2$ exhibits exceptionally higher initial activity (~90 % and ~94 % for $CH_4$ and $CO_2$, respectively, which are closer to equilibrium conversions $CH_4$ = 98.3 % and $CO_2$ = 99.1 %) and the conversions and $H_2$/CO ratio (Fig. 1c,d and Fig. 2b) are kept stable in the test time range (14 h).

Actually, $CO_2$-pretreated Rh/$CeO_2$ catalyst exhibits superior catalytic performance in a wide reaction temperature ranging from 600 to 850 °C than others such as Rh/$CeO_2$-200-$H_2$ and Rh/$CeO_2$-850-$H_2$, with dramatically high conversion of methane and $CO_2$ at a fixed temperature. For example, the conversions of $CH_4$ and $CO_2$ over Rh/$CeO_2$-850-$CO_2$ are 74.1% and 90.9% at 750 °C , respectively. Meanwhile, the conversions of $CH_4$ and $CO_2$ over Rh/$CeO_2$-200-$H_2$ and Rh/$CeO_2$-850-$H_2$ are only 5.4%, 20.3%, 0.78% and 12.8%, respectively, Fig. 3. In addition, in the long-term stability test of the DRM reaction, the conversion of methane and $CO_2$ is below 92 % and 97 %, respectively, which are both lower than the equilibrium values (Fig. 4a). The stability test shows that Rh/$CeO_2$-850-$CO_2$ exhibits nearly stable performance in a 100-hour test (only 2.5 % decrease in $CH_4$ conversion). After 100-hour test, TG-Mass analysis of the sample of Rh/$CeO_2$-850-$CO_2$ shown no detectable carbon accumulation (Fig. S1). To exclude the possibility that this unusual phenomenon was caused by the commercial $CeO_2$ that may contain any impurity, we used homemade $CeO_2$ as support with similar specific surface area compared with commercial $CeO_2$ support (Table S2) which resulted in a simialr Rh states (Fig. S2), and the sample also exhibited similar trend (Fig. 4b), suggesting that this phenomenon is general.

The specific activity of Rh/$CeO_2$-850-$H_2$ and Rh/$CeO_2$-850-$CO_2$ catalysts was measured at 850 °C and the corresponding TOF was calculated to compare with literature results. As shown in Table S3, the initial specific activity and turnover frequency (TOF) obtained on Rh/$CeO_2$-850-$H_2$ catalyst at 850 °C are 10.3 mol $g_{Rh}^{-1}$ $h^{-1}$ and 0.48 $s^{-1}$, respectively, which gradually increased with reaction time to 298 mol $g_{Rh}^{-1}$ $h^{-1}$ and 14.0 $s^{-1}$ at 4 h. On the other hand, Rh/$CeO_2$-850-$CO_2$ catalyst exhibits higher and stable specific activity (~ 380 mol $g_{Rh}^{-1}$ $h^{-1}$) and TOF (~20 $s^{-1}$). It is important to note that the specific rate and TOF obtained with Rh/$CeO_2$-850-$CO_2$ catalyst is comparable or higher than the catalysts reported in literatures (Table S4). The above results unambiguously suggest that $CO_2$ treatment has aroused dramatical catalytic performance increase. Therefore, catalyst characterization was performed to try to disclose the underlying reasons.

### 3.2. *Characterization of catalysts structures*

As shown in Fig. S3a, the high-resolution transmission electron

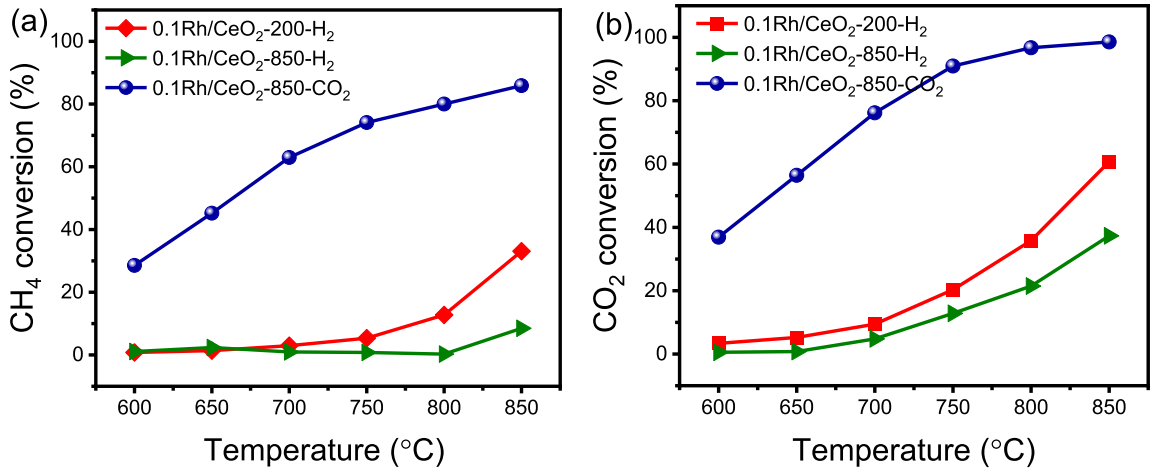


**Fig. 3.** Catalytic performance of $H_2$-treated and $CO_2$-treated Rh/$CeO_2$ catalysts in DRM reaction at different reaction temperatures. (a) $CH_4$ conversion and (b) $CO_2$ conversion. Each conversion point was obtained by waiting for 10 min after the reaction temperature reaching the setting value, i.e., the time-on-stream for each conversion point is 10 min.

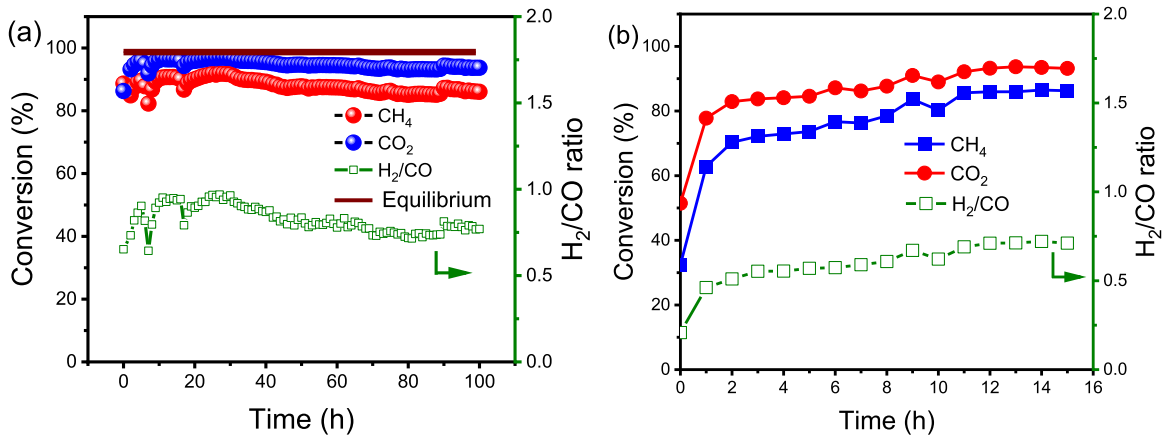


**Fig. 4.** (a) Stability performance of Rh/$CeO_2$-850-$CO_2$ catalyst in DRM reaction at 850 °C. Reaction condition: feed gas = $CH_4$: $CO_2$ = 1, GHSV of 36000 mL $g_{cat}^{-1}$·$h^{-1}$. (b) Catalytic performance of homemade $CeO_2$ supported Rh catalyst in DRM reaction at 850 °C after the catalyst being reduced at 850 °C for 1 h with pure $H_2$, 30 mL/min.

microscopy (HRTEM) image of Rh/$CeO_2$-fresh catalyst shows the presence of highly dispersed Rh cluster with an average size of 0.88 nm. After reduction at 200 °C, Rh clusters aggregated slightly to average size of 1.10 nm, Fig. S3b. However, after high-temperature reduction, as well as $CO_2$ pretreatment (at 850 °C), Rh clusters slightly sintered to a similar size of 1.69 and 1.88 nm, respectively, (Fig. S3c–d). The HRTEM images with higher magnification show that Rh NPs are all bare on Rh/$CeO_2$-fresh sample (Fig. S4a), while on Rh/$CeO_2$-200-$H_2$ catalyst (Fig. S4b–d) a mixture of fully encapsulated, partially encapsulated and bare Rh NPs co-existed. On the other hand, most of the Rh NPs on Rh/$CeO_2$-850-$H_2$ catalysts were encapsulated, (in order to more clearly show the overlayers on Rh NPs surface, we deliberately exhibit the large-sized Rh NPs, Fig. 5a–b). Interestingly, the Rh NPs on Rh/$CeO_2$-850-$CO_2$ (Fig. 5c–d) were also encapsulated. To identify the composition of the encapsulation layer, in-situ electron energy loss spectroscopy (EELS) analysis was further performed. As shown in Fig. 5e–f, the encapsulated Rh NPs on both samples show clear Ce signals (Ce-$M_5$ and Ce-$M_4$ in region II) with an edge slightly lower than that of $CeO_2$ support (region III). In addition, the intensity ratio ($M_5/M_4$, 0.98) is slightly higher than that of $Ce^{4+}$ species (0.82), suggesting that the encapsulation layer is composed of $Ce^{3+}$ species.[47] All these data reveal that reduced ceria (likely $Ce_2O_3$) species migrated onto the surface of Rh NPs on $CO_2$-pretreated and $H_2$-pretreated samples. The HR-TEM images and mean size distribution of Rh NPs in Rh/$CeO_2$-850-$CO_2$ after 100-hour test of DRM reaction shown no dramatically sintering (Fig. S5), which verifies the influence of overlayer encapsulation on catalyst stability (Fig. 4a).

### 3.3. Adsorption properties and electronic state

To determine the influence of encapsulation on adsorption properties and the electronic state of Rh, CO adsorption on Rh/$CeO_2$ catalysts were studied by in-situ diffuse reflectance spectroscopy (CO-DRIFTS) and the results are shown in Fig. 6a. Rh/$CeO_2$-200-$H_2$ shows six peaks at 2084 $cm^{-1}$, 2072 $cm^{-1}$, 2044 $cm^{-1}$, 2020 $cm^{-1}$ 1860 $cm^{-1}$ and 1820 $cm^{-1}$, respectively. Among them, 2084 $cm^{-1}$ and 2020 $cm^{-1}$ bands correspond to *gem*-dicarbonyl species adsorbed on positively charged $Rh^+$ species, while the bands at 2072 $cm^{-1}$ and 2044 $cm^{-1}$ are attributed to linear CO adsorption on electron rich $Rh^+$ species and metallic $Rh^0$, respectively [48–50]. Accordingly, the bands at 1860 $cm^{-1}$ and 1820 $cm^{-1}$ should be assigned to bridged CO adsorption on $Rh^+$ and $Rh^0$ species [48–52]. All these peaks suggested that in this sample Rh existed as mixture of metallic and positively charged states. After being reduced at 850 °C (Rh/$CeO_2$-850-$H_2$), the peak relates to CO adsorption on positively charged Rh species disappeared, suggesting

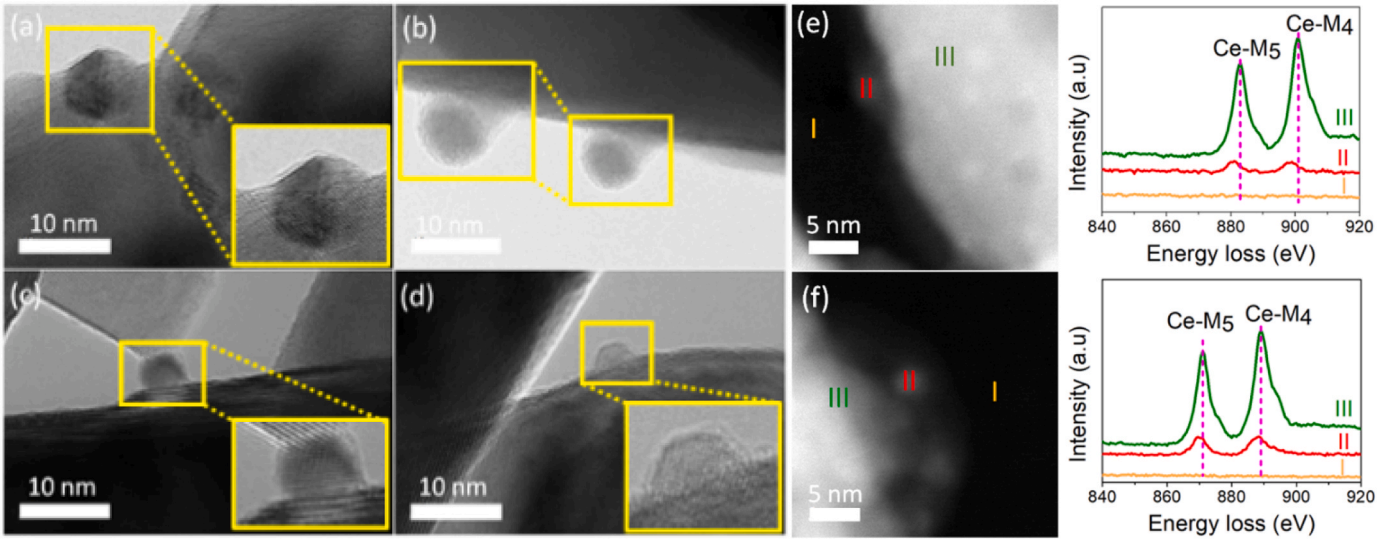


**Fig. 5.** HRTEM images of (a-b) Rh/$CeO_2$-850-$H_2$, (c-d) Rh/$CeO_2$-850-$CO_2$ and in-situ EELS spectra of Ce-$M_{4,5}$ edge of (e) Rh/$CeO_2$-850-$H_2$ and (f) Rh/$CeO_2$-850-$CO_2$ catalysts. Yellow colored boxes highlight encapsulated Rh nanoparticles.

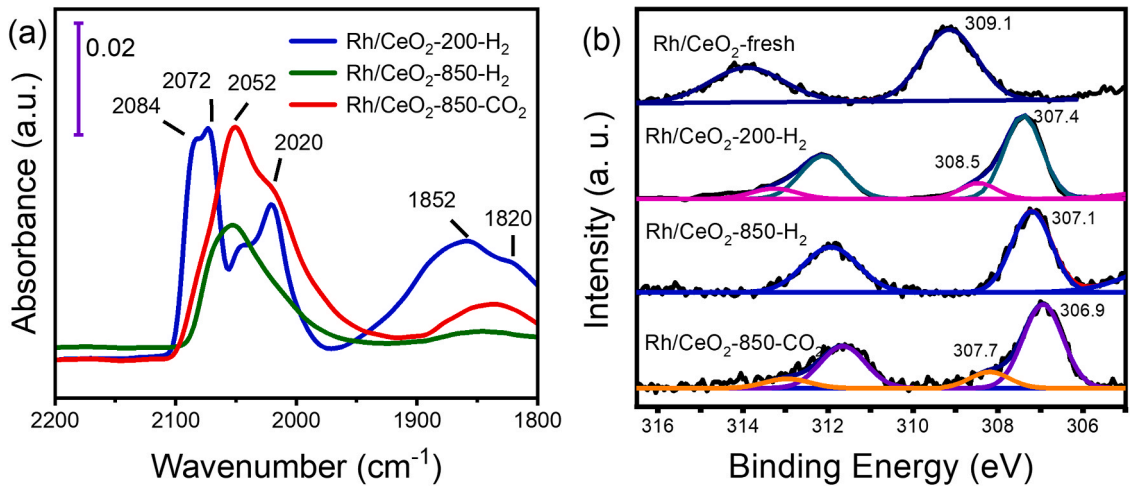


**Fig. 6.** (a) In-situ DRIFTS spectra of CO adsorption on $H_2$-pretreated ($Rh/CeO_2$-200-$H_2$ and $Rh/CeO_2$-850-$H_2$) and $CO_2$-pretreated ($Rh/CeO_2$-850-$CO_2$) catalyst and (b) In-situ XPS spectra of Rh 3d of $Rh/CeO_2$-fresh, $Rh/CeO_2$-850-$H_2$ and $Rh/CeO_2$-850-$CO_2$ catalysts.

that Rh was totally reduced. In addition, the intensity of CO adsorption on $Rh^0$ is significantly suppressed, consistent with the encapsulation of Rh NPs (Fig. 6a). In contrast, after $CO_2$-pretreatment at 850 °C ($Rh/CeO_2$-850-$CO_2$), the intensity of CO adsorption on $Rh^+$ species decreased drastically and a prominent peak for $Rh^0$ species (2052 $cm^{-1}$) appeared, suggesting the existence of metallic Rh along with a small portion of $Rh^+$ species. It should be noted that the intensity of CO adsorption on $Rh^0$ in $Rh/CeO_2$-850-$CO_2$ catalyst is much higher than that in $Rh/CeO_2$-850-$H_2$ catalyst. As $Rh/CeO_2$-850-$CO_2$ catalyst has similar size of Rh with encapsulation layer, its higher CO adsorption suggests that the encapsulation is porous and permeable [35,53].

In-situ X-ray photoelectron spectroscopy (XPS) measurement was carried out to further confirm the Rh chemical state. As shown in Fig. 6b, the Rh $3d_{5/2}$ spectrum of $Rh/CeO_2$-fresh catalyst exhibits a single component with binding energy (BE) of 309.1 eV, indicating that Rh is in + 3 oxidation state [49,54]. However, $Rh/CeO_2$-200-$H_2$ sample shows the presence of two components with BE of 307.4 eV(84.2 %) and 308.5 eV (15.8 %) which are assigned to $Rh^0$ and $Rh^{1+}$ species, respectively, whereas the BE of Rh $3d_{5/2}$ peak at 307.1 eV in 0.1$Rh/CeO_2$-850-$H_2$ catalyst indicates the only existence of metallic $Rh^0$ [55]. One may argue that a reduction treatment with $H_2$ at moderate temperatures can result in a permeable encapsulation layer and the mixture of $Rh^{\delta+}/Rh^0$, achieving the same effect of $CO_2$ pretreatment. However, we conducted tests on the catalytic performance of $Rh/CeO_2$-T-$H_2$ (T = 300–700) under the same reaction conditions and discovered an induction period in the catalytic activity of all $Rh/CeO_2$-T-$H_2$ samples, regardless of the pretreatment temperature (Fig. S6). The existence of the induction period indicates that a reduction treatment with $H_2$ at moderate temperatures resulting in a permeable encapsulation layer cannot achieve the same effect induced by $CO_2$ pretreatment under high temperatures. To explore the underlying reason for the induction period of $Rh/TiO_2$-T-$H_2$ (T = 300–700), CO adsorption on $Rh/CeO_2$-T-$H_2$ (T = 300–700) was studied with in situ CO-DRIFT. The frequency of CO stretching vibration on $Rh/CeO_2$-300-$H_2$, $Rh/CeO_2$-400-$H_2$, and $Rh/CeO_2$-500-$H_2$ are similar to that of $Rh/CeO_2$-850-$H_2$, which confirmed the metallic Rh species in samples of $Rh/CeO_2$-300-$H_2$, $Rh/CeO_2$-400-$H_2$, $Rh/CeO_2$-500-$H_2$, and $Rh/CeO_2$-850-$H_2$ (Fig. S7). Thus, the difference in initial activity of DRM reaction between $Rh/CeO_2$-850-$CO_2$ and $Rh/CeO_2$-T-$H_2$ (T = 300–700) is attributed to their electronic structure. On the other hand, the Rh $3d_{5/2}$ peak in $Rh/CeO_2$-850-$CO_2$ catalyst shows two peaks positioned at 306.9 eV (84.3 %) and 307.7 eV (15.7 %), also assigned to $Rh^0$ and $Rh^{\delta+}$ species [56,57]. However, it shows clearly that the positions for both peaks are lower than that on $Rh/CeO_2$-200-$H_2$ (0.5 and 0.8 eV lower, respectively). Therefore, the in-situ XPS results refer clearly that the chemical state of Rh on $Rh/CeO_2$-850-$CO_2$ is special and different from those on other samples, consistent well with in-situ CO-DRIFTS result.

### 3.4. Temperature programmed surface reaction

The significantly increased initial activity in DRM after $CO_2$ treatment should come from increased $CH_4$ activation which is ofter regarded as the rate-determining step in this reaction. To confirm this, $CH_4$ decomposition experiment (1 vol% $CH_4$/He) was conducted on $Rh/CeO_2$-850-$H_2$ and $Rh/CeO_2$-850-$CO_2$ catalysts at 600 °C. As shown in Fig. S8, $Rh/CeO_2$-850-$CO_2$ catalyst exhibits much higher (five folds) initial $CH_4$ conversion (60 %) than $Rh/CeO_2$-850-$H_2$ (12 %) in $CH_4$ decomposition reaction. Considering the fact that in-situ CO-DRIFTS result (Fig. 6a) shows that $Rh/CeO_2$-850-$CO_2$ catalyst has only two times CO adsorption amount of that of $Rh/CeO_2$-850-$H_2$ catalyst, other factors in addition to permeable encapsulation layer must have accounted for the higher initial activity. Wang et al. reported that the presence of $CeO_2$ in $Rh/CeO_2$-$Al_2O_3$ catalyst generates $Rh^{\delta+}/Rh^0$ redox couple and the electron-deficient $Rh^{\delta+}$ sites are considered to promote the dissociation of the C-H bond in methane by accepting σ electrons from C-H bond, resulting in increased $CH_4$ conversion [57]. To confirm further rate determining step, temperature programmed surface reaction (TPSR) with MS of $CH_4$ decomposition carried out on $Rh/CeO_2$-850-$CO_2$ and $Rh/CeO_2$-850-$H_2$ catalysts. As shown in the Fig. 7a, the formation of CO and $H_2$ is observed at 550 °C on $Rh/CeO_2$-850-$H_2$ in $CH_4$TPSR experiments. Surprisingly, when $Rh/CeO_2$ sample is pretreated with $CO_2$ at 850 °C, the temperature of CO and $H_2$ formation is reduced to 315 °C (Fig. 7b), which clearly confirmed the great enhancement in $CH_4$ activation via $CO_2$ treatment at high temperature. Based on the CO-DRIFTS, XPS and $CH_4$-TPSR results, we therefore believe that the higher activity of $Rh/CeO_2$-850-$CO_2$ catalyst should originate from the presence of both $Rh^{\delta+}/Rh^0$ species and permeable encapsulation layer by $CO_2$ treatment.

One may argue that the subtle $Rh^{\delta+}/Rh^0$ combination cannot be maintained during the high-temperature DRM reaction. In-situ CO-DRIFT examination was performed after operando DRM reaction at 700 °C. It shows that the spent-$Rh/CeO_2$-850-$CO_2$ catalyst after 3-hour reaction shows almost the same CO absorption to that of the $Rh/CeO_2$-850-$CO_2$ (Fig. S9), suggesting the subtle chemical state mixture can be maintained upon reaction. The catalytic performance test shows that at 700 °C the initial activity is also high and stable (Fig. S10).

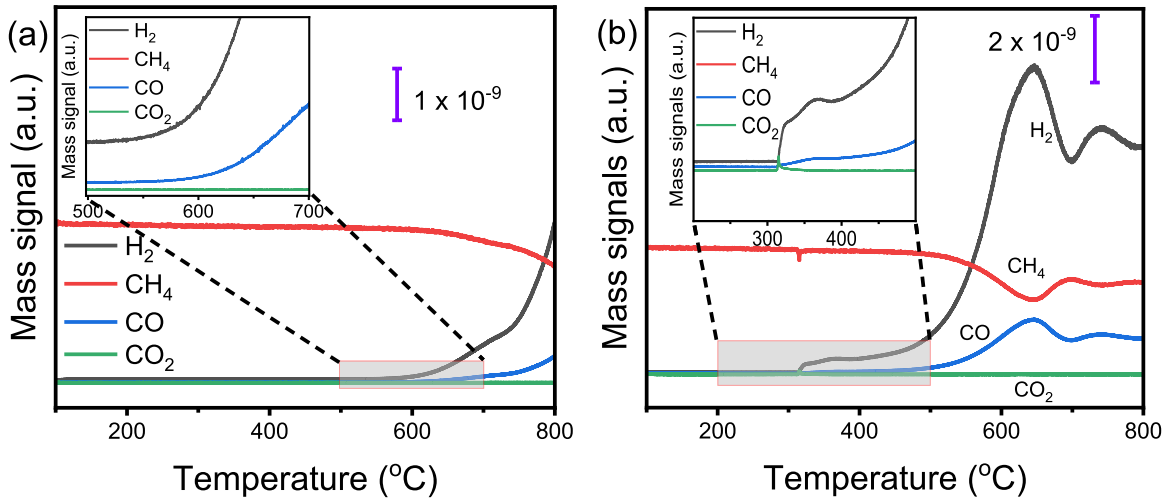


**Fig. 7.** The temperature programmed surface reaction (TPSR) of methane over Rh/$CeO_2$-850-$H_2$ (a) and Rh/$CeO_2$-850-$CO_2$ (b). Reaction condition: 1 vol% $CH_4$/He, GHSV= 36000 mL $g{\cdot}cat^{-1}{\cdot}h^{-1}$.

### 3.5. $CO_2$ and CO DRIFTS

The driving force for the formation of $CO_2$-SMSI and the subtle $Rh^{\delta+}$/$Rh^0$ combination is believed to stem from the co-effect of CO and O resulted from the dissociation of $CO_2$ since $CO_2$ itself is almost inert. To confirm this, in situ $CO_2$-DRIFT spectra was recorded on Rh/$CeO_2$-fresh catalyst under $CO_2$ gas flow at different temperatures. As shown in Fig. 8a, at room temperature (RT), it shows a linear CO adsorption on $Rh^+$ at 2077 $cm^{-1}$ [48], revealing that $CO_2$ dissociation even occurs at RT. With temperature increasing, *gem*-dicarbonyl CO adsorption appears as well. Further increasing the temperature to 500 °C, the intensity of both CO adsorption peaks decreases along with the appearance of gaseous CO due to the CO desorption. It should be noted that CO adsorption is still observable at 500 °C. For comparison, CO adsorption on same sample was performed with same procedure and it shows a similar trend, Fig. 8b. However, at 500 °C there is almost no CO adsorption due to the CO induced SMSI. Therefore, it suggests that CO can indeed induce SMSI which is, however, different from that with the presence of O. Therefore, $CO_2$ treatment is certainly special and can induce slightly different state of SMSI. In addition, this set of experiments also suggest that the $CO_2$ induced SMSI might be different from the recently reported $CO_2$-induced SMSI through Le Chatelier's principle [34,58]. Besides, the XRD patterns of Rh/$CeO_2$-850-$CO_2$ shows no diffraction peaks of $Ce_2(CO_3)_3$, which further excludes the possibility of $CO_2$-induced SMSI in Rh/$CeO_2$ through Le Chatelier's principle (Fig. S11).

The above results unambiguously demonstrate that SMSI can occur upon $CO_2$-treatment at high temperatures. The resultant subtle mixture of $Rh^{\delta+}$/$Rh^0$ is critical in improving $CH_4$ activation, whereas the presence of penetrable encapsulation layer is favorable for providing more active sites, thus giving rise to a significantly enhanced DRM activity. Of more importance, this finding can be extended to other metal such as ruthenium. As shown in Fig. S12, Ru/$CeO_2$ catalyst exhibits similar phenomenon. However, the increase of initial DRM activity is not observed on Rh supported over other metal oxides such as $TiO_2$ and $Al_2O_3$ (Fig. S13), which is due to the support-dependency of $CO_2$ induced SMSI.

## 4. Conclusion

In summary, the present study demonstrates the SMSI between Rh NPs and $CeO_2$ support can be operando formed under DRM reaction by $CO_2$ molecules. The Rh/$CeO_2$ catalyst with $CO_2$-SMSI state exhibits much higher initial activity than classical SMSI catalyst and non-SMSI

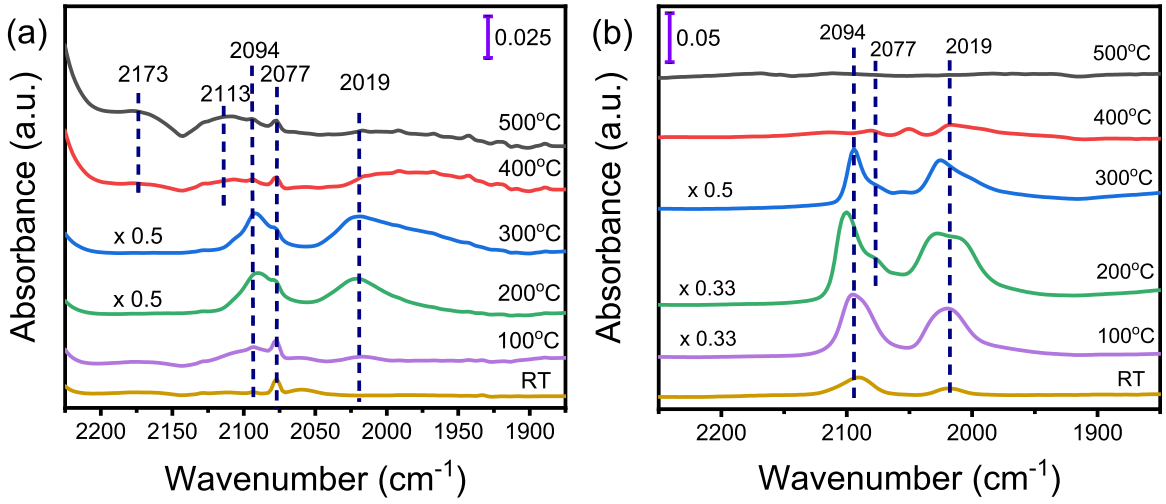


**Fig. 8.** (a) $CO_2$-DRIFT spectra of Rh/$CeO_2$-fresh catalyst recorded in the flow of $CO_2$ gas at different temperatures and (b) CO-DRIFT spectra of Rh/$CeO_2$-fresh catalyst recorded at different temperature (the spectra were recorded after the gaseous CO was removed by He purge).

catalyst in DRM reaction. The co-existence of suitable $Rh^{\delta+}/Rh^0$ mixture along with permeable encapsulation layer are responsible for the exceptional activity of $CO_2$-SMSI catalyst in DRM reaction. The finding is general and can be extended to other metals. We believe that $CO_2$ pretreatment is a promising strategy to alter the metal-support interactions as well as metal electronic properties, and subsequently tune catalytic activity.

## Credit authorship contribution statement

Y.G., and F.H. contributed equally. Y.G. and F.H. performed the catalyst synthesis, catalytic experiments, conducted some characterization and wrote the original draft. Q.L. and Y.S. performed the HRTEM analysis, W.L. performed the in-situ EELS experiments, X.J. and L.L. performed the in-situ CO-DRIFTS experiments. M.A. participated in the data analysis. B.Q. L.L. and Y.Z. conceived the idea, supervised the project. B.Q., L.L. and Y.Z. revised the manuscript. All authors are discussed the result and commented on the manuscript, and approved the submission.

## Declaration of Competing Interest

The authors declare that they have no known competing financial interests or personal relationships that could have appeared to influence the work reported in this paper.

## Data Availability

Data will be made available on request.

## Acknowledgments

This work was financially supported by National Key Research and Development Program of China (2021YFA1500503), National Natural Science Foundation of China (21972135, 21961142006, 22090033 and 51701201), and CAS Project for Young Scientists in Basic Research (YSBR-022).

## Appendix A. Supporting information

Supplementary data associated with this article can be found in the online version at doi:10.1016/j.apcatb.2023.123503.

## References

[1] L. Zhang, X. Wang, C. Chen, X. Zou, X. Shang, W. Ding, X. Lu, Investigation of mesoporous $NiAl_2O_4$/MOx (M = La, Ce, Ca, Mg)–γ-$Al_2O_3$ nanocomposites for dry reforming of methane, RSC Adv. 7 (2017) 33143–33154.
[2] S. Dama, S.R. Ghodke, R. Bobade, H.R. Gurav, S. Chilukuri, Active and durable alkaline earth metal substituted perovskite catalysts for dry reforming of methane, Appl. Catal. B: Environ. 224 (2018) 146–158.
[3] H. Liu, X. Meng, T.D. Dao, H. Zhang, P. Li, K. Chang, T. Wang, M. Li, T. Nagao, J. Ye, Conversion of carbon dioxide by methane reforming under visible-light irradiation: surface-plasmon-mediated nonpolar molecule activation, Angew. Chem. Int Ed. Engl. 54 (2015) 11545–11549.
[4] K. Wittich, M. Krämer, N. Bottke, S.A. Schunk, Catalytic dry reforming of methane: insights from model systems, ChemCatChem 12 (2020) 2130–2147.
[5] M. Akri, S. Zhao, X. Li, K. Zang, A.F. Lee, M.A. Isaacs, W. Xi, Y. Gangarajula, J. Luo, Y. Ren, Y.-T. Cui, L. Li, Y. Su, X. Pan, W. Wen, Y. Pan, K. Wilson, L. Li, B. Qiao, H. Ishii, Y.-F. Liao, A. Wang, X. Wang, T. Zhang, Atomically dispersed nickel as coke-resistant active sites for methane dry reforming, Nat. Commun. 10 (2019) 5181.
[6] R. Zhou, M. Mohamedali, Y. Ren, Q. Lu, N. Mahinpey, Facile synthesis of multi-layered nanostructured $Ni/CeO_2$ catalyst plus in-situ pre-treatment for efficient dry reforming of methane, Appl. Catal. B: Environ. 316 (2022), 121696.
[7] X. Zhang, J. Deng, M. Pupucevski, S. Impeng, B. Yang, G. Chen, S. Kuboon, Q. Zhong, K. Faungnawakij, L. Zheng, G. Wu, D. Zhang, High-performance binary Mo–Ni catalysts for efficient carbon removal during carbon dioxide reforming of methane, ACS Catal. 11 (2021) 12087–12095.
[8] J. Deng, K. Bu, Y. Shen, X. Zhang, J. Zhang, K. Faungnawakij, D. Zhang, Cooperatively enhanced coking resistance via boron nitride coating over Ni-based catalysts for dry reforming of methane, Appl. Catal. B: Environ. 302 (2022), 120859.
[9] D.G. Araiza, F. González-Vigi, A. Gómez-Cortés, J. Arenas-Alatorre, G. Díaz, Pt-based catalysts in the dry reforming of methane: effect of support and metal precursor on the catalytic stability, J. Mex. Chem. Soc. (65) (2021).
[10] Z. Liu, F. Zhang, N. Rui, X. Li, L. Lin, L.E. Betancourt, D. Su, W. Xu, J. Cen, K. Attenkofer, H. Idriss, J.A. Rodriguez, S.D. Senanayake, Highly active ceria-supported Ru catalyst for the dry reforming of methane: in situ identification of $Ru^{\delta+}$–$Ce^{3+}$ interactions for enhanced conversion, ACS Catal. 9 (2019) 3349–3359.
[11] M. Steib, Y. Lou, A. Jentys, J.A. Lercher, Enhanced activity in methane dry reforming by carbon dioxide induced metal-oxide interface restructuring of nickel/zirconia, ChemCatChem 9 (2017) 3809–3813.
[12] N. Yan, Ni-Ir/$MgAl_2O_4$ for balanced carbon deposition-elimination in methane dry reforming, Chem. Catal. 2 (2022) 1520–1521.
[13] S. Liu, C. Dun, M. Shah, J. Chen, S. Rao, J. Wei, E.A. Kyriakidou, J.J. Urban, M. T. Swihart, Producing ultra stable Ni-$ZrO_2$ nanoshell catalysts for dry reforming of methane by flame synthesis and Ni exsolution, Chem. Catal. 2 (2022) 2262–2274.
[14] H. Li, C. Hao, J. Tian, S. Wang, C. Zhao, Ultra-durable Ni-Ir/$MgAl_2O_4$ catalysts for dry reforming of methane enabled by dynamic balance between carbon deposition and elimination, Chem. Catal. 2 (2022) 1748–1763.
[15] Z. Hu, L. Zhang, Catalytic activity of bimetallic Rh/Rh-M nanosheets governed by CO spillover, Chem. Catal. 2 (2022) 1512–1514.
[16] Jing Sixue Lin, Yangyang Wang, Senyou Mi, Zheng Yang, Wenming Wang, Daishe Wu Liu H., Peng, Trifunctional strategy for the design and synthesis of a Ni-$CeO_2$@$SiO_2$ catalyst with remarkable low-temperature sintering and coking resistance for methane dry reforming, Chin. J. Catal. 42 (2021) 1808–1820.
[17] S. Kweon, Y.W. Kim, D. Jo, C.-H. Shin, M.B. Park, H.-K. Min, Defect-induced formation of nickel silicates on two-dimensional MWW-type catalysts promoting catalytic activity for dry reforming of methane, Microporous Mesoporous Mater. 332 (2022), 111683.
[18] X. Feng, J. Liu, P. Zhang, Q. Zhang, L. Xu, L. Zhao, X. Song, L. Gao, Highly coke resistant Mg–Ni/$Al_2O_3$ catalyst prepared via a novel magnesiothermic reduction for methane reforming catalysis with $CO_2$: the unique role of Al–Ni intermetallics, Nanoscale 11 (2019) 1262–1272.
[19] S. Arora, R. Prasad, An overview on dry reforming of methane: strategies to reduce carbonaceous deactivation of catalysts, RSC Adv. 6 (2016) 108668–108688.
[20] P. Djinović, J. Batista, A. Pintar, Efficient catalytic abatement of greenhouse gases: Methane reforming with $CO_2$ using a novel and thermally stable Rh–$CeO_2$ catalyst, Int. J. Hydrog. Energy 37 (2012) 2699–2707.
[21] J. Wu, L.-Y. Qiao, Z.-F. Zhou, G.-J. Cui, S.-S. Zong, D.-J. Xu, R.-P. Ye, R.-P. Chen, R. Si, Y.-G. Yao, Revealing the synergistic effects of Rh and substituted $La_2B_2O_7$ (B = Zr or Ti) for preserving the reactivity of catalyst in dry reforming of methane, ACS Catal. 9 (2019) 932–945.
[22] K. Shimura, T. Fujitani, Effects of rhodium catalyst support and particle size on dry reforming of methane at moderate temperatures, Mol. Catal. 509 (2021), 111623.
[23] Z.L. Zhang, V.A. Tsipouriari, A.M. Efstathiou, X.E. Verykios, Reforming of methane with carbon dioxide to synthesis gas over supported rhodium catalysts: I. Effects of support and metal crystallite size on reaction activity and deactivation characteristics, J. Catal. 158 (1996) 51–63.
[24] D. Pakhare, J. Spivey, A review of dry ($CO_2$) reforming of methane over noble metal catalysts, Chem. Soc. Rev. 43 (2014) 7813–7837.
[25] H.Y. Wang, E. Ruckenstein, Carbon dioxide reforming of methane to synthesis gas over supported rhodium catalysts: the effect of support, Appl. Catal. A: Gen. 204 (2000) 143–152.
[26] S.J. Tauster, S.C. Fung, R.T.K. Baker, J.A. Horsley, Strong interactions in supported-metal catalysts, Science 211 (1981) 1121–1125.
[27] J. Zhang, H. Wang, L. Wang, S. Ali, C. Wang, L. Wang, X. Meng, B. Li, D.S. Su, F. S. Xiao, Wet-chemistry strong metal-support interactions in titania-supported Au catalysts, J. Am. Chem. Soc. 141 (2019) 2975–2983.
[28] H. Tang, Y. Su, B. Zhang, A.F. Lee, M.A. Isaacs, K. Wilson, L. Li, Y. Ren, J. Huang, M. Haruta, B. Qiao, X. Liu, C. Jin, D. Su, J. Wang, T. Zhang, Classical strong metal-support interactions between gold nanoparticles and titanium dioxide, Sci. Adv. 3 (2017), e1700231.
[29] B. Han, Y. Guo, Y. Huang, W. Xi, J. Xu, J. Luo, H. Qi, Y. Ren, X. Liu, B. Qiao, T. Zhang, Strong metal-support interactions between Pt single atoms and $TiO_2$, Angew. Chem. Int Ed. Engl. 59 (2020) 11824–11829.
[30] H. Xin, L. Lin, R. Li, D. Li, T. Song, R. Mu, Q. Fu, X. Bao, Overturning $CO_2$ hydrogenation selectivity with high activity via reaction-induced strong metal–support interactions, J. Am. Chem. Soc. 144 (2022) 4874–4882.
[31] E.D. Goodman, A.S. Asundi, A.S. Hoffman, K.C. Bustillo, J.F. Stebbins, S.R. Bare, S. F. Bent, M. Cargnello, Monolayer support control and precise colloidal nanocrystals demonstrate metal–support interactions in heterogeneous catalysts, Adv. Mater. 33 (2021) 2104533.
[32] S. Bernal, J.J. Calvino, M.A. Cauqui, G.A. Cifredo, A. Jobacho, J.M. Rodríguez-Izquierdo, Metal-support interaction phenomena in rhodium/ceria and rhodium/titania catalysts: comparative study by high-resolution transmission electron spectroscopy, Appl. Catal. A: Gen. 99 (1993) 1–8.
[33] X. Du, Y. Huang, X. Pan, B. Han, Y. Su, Q. Jiang, M. Li, H. Tang, G. Li, B. Qiao, Size-dependent strong metal-support interaction in $TiO_2$ supported Au nanocatalysts, Nat. Commun. 11 (2020) 5811.
[34] H. Wang, L. Wang, D. Lin, X. Feng, Y. Niu, B. Zhang, F.-S. Xiao, Strong metal–support interactions on gold nanoparticle catalysts achieved through Le Chatelier's principle, Nat. Catal. 4 (2021) 418–424.
[35] J. Zhang, D. Zhu, J. Yan, C.-A. Wang, Strong metal-support interactions induced by an ultrafast laser, Nat. Commun. 12 (2021) 6665.

[36] J.C. Matsubu, S. Zhang, L. DeRita, N.S. Marinkovic, J.G. Chen, G.W. Graham, X. Pan, P. Christopher, Adsorbate-mediated strong metal–support interactions in oxide-supported Rh catalysts, Nat. Chem. 9 (2017) 120–127.
[37] J. Dong, Q. Fu, H. Li, J. Xiao, B. Yang, B. Zhang, Y. Bai, T. Song, R. Zhang, L. Gao, J. Cai, H. Zhang, Z. Liu, X. Bao, Reaction-induced strong metal–support interactions between metals and inert boron nitride nanosheets, J. Am. Chem. Soc. 142 (2020) 17167–17174.
[38] J. Zhang, J. Ma, T.S. Choksi, D. Zhou, S. Han, Y.-F. Liao, H.B. Yang, D. Liu, Z. Zeng, W. Liu, X. Sun, T. Zhang, B. Liu, Strong metal–support interaction boosts activity, selectivity, and stability in electrosynthesis of $H_2O_2$, J. Am. Chem. Soc. 144 (2022) 2255–2263.
[39] H. Tang, Y. Su, Y. Guo, L. Zhang, T. Li, K. Zang, F. Liu, L. Li, J. Luo, B. Qiao, J. Wang, Oxidative strong metal–support interactions (OMSI) of supported platinum-group metal catalysts, Chem. Sci. 9 (2018) 6679–6684.
[40] N. Rui, X. Wang, K. Deng, J. Moncada, R. Rosales, F. Zhang, W. Xu, I. Waluyo, A. Hunt, E. Stavitski, S.D. Senanayake, P. Liu, J.A. Rodriguez, Atomic structural origin of the high methanol selectivity over $In_2O_3$–metal interfaces: metal–support interactions and the formation of a InOx overlayer in $Ru/In_2O_3$ catalysts during $CO_2$ hydrogenation, ACS Catal. 13 (2023) 3187–3200.
[41] T. Song, J. Dong, R. Li, X. Xu, M. Hiroaki, B. Yang, R. Zhang, Y. Bai, H. Xin, L. Lin, R. Mu, Q. Fu, X. Bao, Oxidative strong metal–support interactions between metals and inert boron nitride, J. Phys. Chem. Lett. 12 (2021) 4187–4194.
[42] H. Tang, J. Wei, F. Liu, B. Qiao, X. Pan, L. Li, J. Liu, J. Wang, T. Zhang, Strong metal–support interactions between gold nanoparticles and nonoxides, J. Am. Chem. Soc. 138 (2016) 56–59.
[43] X. Liu, M.-H. Liu, Y.-C. Luo, C.-Y. Mou, S.D. Lin, H. Cheng, J.-M. Chen, J.-F. Lee, T.-S. Lin, Strong metal–support interactions between gold nanoparticles and ZnO nanorods in CO oxidation, J. Am. Chem. Soc. 134 (2012) 10251–10258.
[44] F. Polo-Garzon, T.F. Blum, Z. Bao, K. Wang, V. Fung, Z. Huang, E.E. Bickel, D.-e Jiang, M. Chi, Z. Wu, In situ strong metal–support interaction (SMSI) affects catalytic alcohol conversion, ACS Catal. 11 (2021) 1938–1945.
[45] H. Tang, F. Liu, J. Wei, B. Qiao, K. Zhao, Y. Su, C. Jin, L. Li, J.J. Liu, J. Wang, T. Zhang, Ultrastable hydroxyapatite/titanium-dioxide-supported gold nanocatalyst with strong metal-support interaction for carbon monoxide oxidation, Angew. Chem. Int. Ed. Engl. 55 (2016) 10606–10611.
[46] S. Liu, W. Xu, Y. Niu, B. Zhang, L. Zheng, W. Liu, L. Li, J. Wang, Ultrastable Au nanoparticles on titania through an encapsulation strategy under oxidative atmosphere, Nat. Commun. 10 (2019) 5790.
[47] S.M. Collins, S. Fernandez-Garcia, J.J. Calvino, P.A. Midgley, Sub-nanometer surface chemistry and orbital hybridization in lanthanum-doped ceria nano-catalysts revealed by 3D electron microscopy, Sci. Rep. 7 (2017) 5406.
[48] H. Zhu, Y. Li, X. Zheng, In-situ DRIFTS study of $CeO_2$ supported Rh catalysts for $N_2O$ decomposition, Appl. Catal. A: Gen. 571 (2019) 89–95.
[49] L. Li, M. Chu, R. Song, S. Liu, G. Ren, Y. Xu, L. Wang, Q. Xu, Q. Shao, J. Lu, X. Huang, CO spillover on ultrathin bimetallic Rh/Rh-M nanosheets, Chem. Catal. 2 (2022) 1709–1719.
[50] Nhung N. Duong, Darius Aruho, Bin Wang, D.E. Resasco, Hydrodeoxygenation of anisole over different Rh surfaces, Chin. J. Catal. 40 (2019) 1721–1730.
[51] D.I. Kondarides, Z. Zhang, X.E. Verykios, Chlorine-induced alterations in oxidation state and CO chemisorptive properties of $CeO_2$-supported Rh catalysts, J. Catal. 176 (1998) 536–544.
[52] C. Larese, M.L. Granados, F.C. Galisteo, R. Mariscal, J.L.G. Fierro, TWC deactivation by lead: a study of the $Rh/CeO_2$ system, Appl. Catal. B: Environ. 62 (2006) 132–143.
[53] A. Nakayama, R. Sodenaga, Y. Gangarajula, A. Taketoshi, T. Murayama, T. Honma, N. Sakaguchi, T. Shimada, S. Takagi, M. Haruta, B. Qiao, J. Wang, T. Ishida, Enhancement effect of strong metal-support interaction (SMSI) on the catalytic activity of substituted-hydroxyapatite supported Au clusters, J. Catal. 410 (2022) 194–205.
[54] C. Force, E. Roman, J.M. Guil, J. Sanz, XPS and $^1$H NMR study of thermally stabilized $Rh/CeO_2$ catalysts submitted to reduction/oxidation treatments, Langmuir 23 (2007) 4569–4574.
[55] S. Yacob, S. Park, B.A. Kilos, D.G. Barton, J.M. Notestein, Vapor-phase ethanol carbonylation with heteropolyacid-supported Rh, J. Catal. 325 (2015) 1–8.
[56] R. Lang, T. Li, D. Matsumura, S. Miao, Y. Ren, Y.T. Cui, Y. Tan, B. Qiao, L. Li, A. Wang, X. Wang, T. Zhang, Hydroformylation of olefins by a rhodium single-atom catalyst with activity comparable to $RhCl(PPh_3)_3$, Angew. Chem. Int. Ed. Engl. 55 (2016) 16054–16058.
[57] R. Wang, H. Xu, X. Liu, Q. Ge, W. Li, Role of redox couples of $Rh^0/Rh^{\delta+}$ and $Ce^{4+}/Ce^{3+}$ in $CH_4/CO_2$ reforming over $Rh–CeO_2/Al_2O_3$ catalyst, Appl. Catal. A: Gen. 305 (2006) 204–210.
[58] X.-W. Liu, D. Ma, Neotype strong metal-support interactions: $CO_2$-induced MgO migration on gold nanoparticles, Chem. Catal. 1 (2021) 29–31.